IJL, Issue 2, Vol. 23, 2024
https://doi.org/10.31900/ijl.v23i2.482

Research Article

IRAQI JOURNAL OF LASER

Enhancement of The Sensitivity of The Refractive Index Sensor Based on D-shaped Coreless Fiber

Dina N. Abdullah*, Hanan J. Taher

Institute of Laser for Postgraduate Studies, University of Baghdad, Baghdad, Iraq
* *Email address of the Corresponding Author: dina.neamat2201m@ilps.uobaghdad.edu.iq*

Article history: Received 5 Jun. 2024; Revised 25 Jul. 2024; Accepted 7 Aug. 2024; Published online 15 Dec. 2024

Abstract: A refractive index sensor has been developed using a D-shaped coreless fiber (DSCF) sensor technique. This sensor comprises a segment of coreless fiber (CF) spliced between two single-mode fibers (SMFs). The middle of the CF length was polished using a grinding wheel to reduce the diameter on one side, creating a D-shaped cross-sectional profile. The DSCF sensor's performance was tested using different concentrations of sodium chloride (NaCl) solutions, with refractive indices (RI) ranging from 1.33 to 1.38. The optimal polishing depth (PD) of 31 µm was determined experimentally, and this was achieved by extending the polishing duration using a grinding wheel. This led to a sensitivity increase from 70.2nm/RIU to 98nm/RIU, meaning the sensitivity increased by 1.4 times. The DSCF sensor is a high-performance, versatile, and cost-effective device with strong interference ability, suitable for various applications.

Keywords: D-shaped coreless fiber (DSCF), refractive index(RI)sensor, coreless fiber (CF), multimode interference (MMI), Mach– Zehnder Interferometer (MZI).

1. Introduction

In a rapidly changing technical world, fiber optic sensors are essential in a wide range of fields such as mechanical, biochemical, biomedical, and spacecraft applications [1–4] to measure physical, chemical, or biological properties due to their excellent sensing and physical properties by examining the wavelength shift, polarization or change in light intensity [5–7]. The optical fiber sensor often incorporates an optical fiber interferometer to measure the phase difference between light beams. There are various layouts of optical interferometers such as Fabry–Perot interferometer , Sagnac fiber interferometer ,Michelson fiber interferometer, and MZI [8–11]. The MZI is the more traditional interferometer to sense RI, concentrations, temperature, and strain because it has versatile flexible geometry and high sensitivity [12–14]. This type of interferometer can be fabricated using various structures, such as the (SMS) structure, which consists of a segment of multimode fiber (MMF) spliced between two single-mode fibers (SMF), or the (SCS) structure involves splicing a CF to act as the sensing part instead of the typical MMF between two SMFs [11]. There are many techniques were used to enhance the sensitivity via increase the evanescent wave leaks from the sensing part(CF) in SCS structure by etching the CF [15] , utilizing offset optical fiber [16], heating and tapering a CF-SMF[17,18] or by removing a layer from one side of the CF to obtain the DSCF [19,20].

D-shaped optical fibers are manufactured using various methods such as chemical etching, laser ablation, and mechanical polishing [15,19,21] .Sensors based on D-shaped optical fiber were developed in two ways , the first was without the need for splicing and used only one type of fiber, such as MMF which showed relatively high sensitivity [22,23]. Another type of sensor based on the D-shape was designed using a structure consisting of photonic crystal fiber (PCF) or coreless fiber as the sensing part [19,24,25]. In addition, a D-shaped sensor was fabricated using plastic optical fiber core for an expanded RI measurements [26]. The SCS MZI structure was used in this paper utilizing the grinding wheel to side-polish the CF to enhance the structure's sensitivity and then attain DSCF sensor for the RIs measurement .Also, the optimal depth was determined by extending the polishing process duration through three experimental tests.

2. The principles of the DSCF sensor

The SCS-MZI interferometer used in this work comprises of two splicing regions, the first splicing region represents a beam splitter coupler where the light enters and splits into two beams, the reference beam travels into the core of the CF, while the sensing beam is guided by air or another medium, with the condition that RI of the ambient environment is lower than the RI of the CF to ensure that the principle of total internal reflection is achieved and the second splicing region is represented a combiner where the reference beam recombined with the sensing beam at the second splicing region causes interference that is represented in Fig.1which shows the SCS structure .The changing in length and diameter of CF caused changing in the sensitivity and the peak spectral response of CF according to MMI theory that was caused by the self-imaging effect can be calculated by using Eq.1 [27–29].

$$\lambda o = P(n_{CF} D_{2CF}/L_{CF}) \quad (1)$$

nCF and DCF were the RI and the diameter of the CF segment in the SCS proposed sensor, respectively and P acts as the self-imaging number which means constructive interference number.

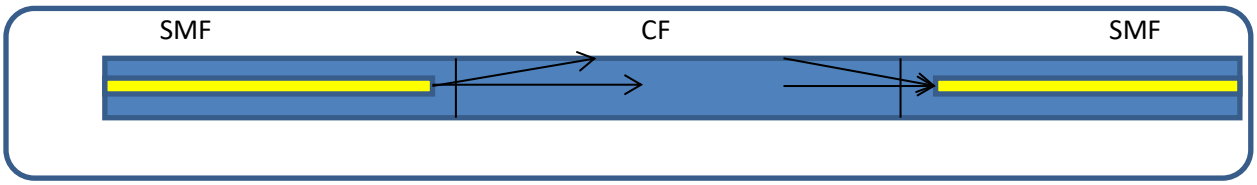

Fig.1: Schematic of in line MZI with inner couplers SCS structure

The principle of the DSCF sensor enhances sensitivity by reducing the distance between the CF and analytes by polishing one side of a coreless fiber. As the polishing deepens, the evanescent wave strength increases, allowing for more precise measurements. The RI of the external environment is determined by changes in transmitted light power or wavelength shifts. Increasing the polishing depth decreases the output intensity. As shown in Fig .2, there are five sections in the DSCF structure: lead in SMF, transitional length (L1), coreless flat section (CFL), transitional length (L2), and lead out SMF. The light inputs from the lead in SMF into the CF divide into two divisions, one of which is transmitted in the air in L1 and the other is coupled to the CFL. The CFL works as a multimode waveguide. The L1 provides an efficient way to excite the high-order modes and strong evanescent waves of the CFL multimode waveguide, which enhances the RI sensitivity. Then the light is recollected from the CFL by the fiber core in the L2 section for output measurement. This technique is based on the interaction between the evanescent wave of the surface of the D-shaped fiber and the external environment resulting in optical transmission attenuation. In other words, The optical transmission structure can be disrupted by reducing the diameter of the optical fiber on one side that disruption allows for the excitation of higher order modes, which in turn brings the fiber core in closer proximity to the measured physical quantity [19,20].

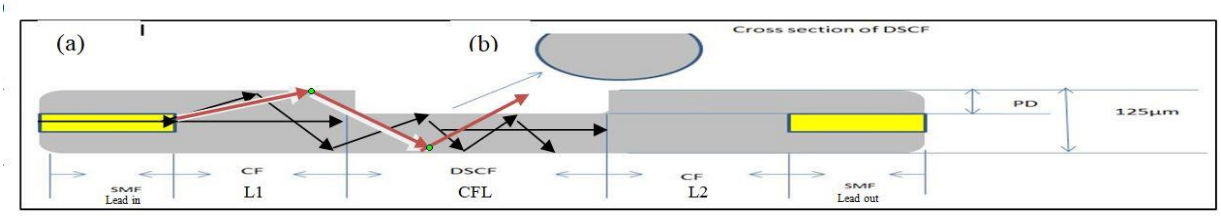

Fig2: Schematic diagrams of (DSCF) (a) vertical section, and (b).cross section of DSCF

This adjustment facilitates more precise and accurate measurements. The RI of the external environment (analyst) is measured by detecting the change in transmitted light power or the shift in wavelength. The RI sensing characteristics of three fabricated DSCFs with different PDs based on the percentage of output intensity of DSCFs were experimentally investigated by extending the duration. It is also clear that as the PD increases, the evanescent field becomes stronger.

3. Materials and method

3.1 The fabrication and characterization of SCS sensing structure

SCS structure was fabricated by splicing a single segment of 6cm long of CF [30,31] with a uniform RI of 1.46 and a diameter of 125 µm (Thorlabs) between two single-mode fibers (SMF-28) with an RI of 1.451 for the core and 1.444 for the cladding by an optical fiber arc fusion splicer (FSM-60S) to create the SCS structure. To prepare the fibers for the splicing process, the outer coating of the CF and 2 cm from the end of the SMFs were stripped using an optical fiber stripper. Then, the fiber terminations of SMFs and CF were cut at a right angle using an optical fiber cleaver (CT-30), this precise cut ensures proper alignment during splicing. After that, SMF was spliced with CF using an optical fiber arc fusion splicer, the splice mode was auto SM/NZ/DS/MM and the heater mode was 60 mm FP-03. Finally, the other end of CF was spliced to the other SMF in a similar manner. Fig.3 illustrates (a) a schematic diagram of the SCS structure and (b) the transmission spectrum (reference) of the SCS structure measured by an optical spectrum analyzer (OSA).

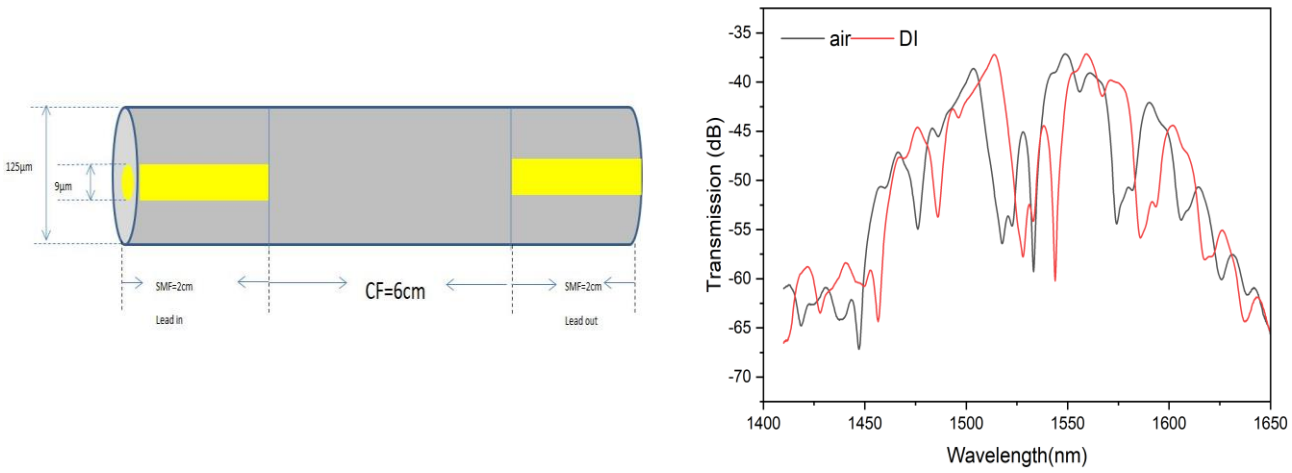

(a) **(b)**

Fig.3: SCS MZI structure (a)schematic diagram of SCS structure(b)transmission spectrum of SCS structure.

3.2 The fabrication and characterization of the DSCF sensing structure

The SCS sensor was initially fixed onto a holder fiber from the SMFs at both ends. One end of the SMF was connected to a 635 nm laser diode (Thorlabs), while the other end of the second SMF was connected to a visible spectrometer (CCS series spectrometer-Thorlabs) with a wavelength range of 350-700 nm as shown below in Fig.4.

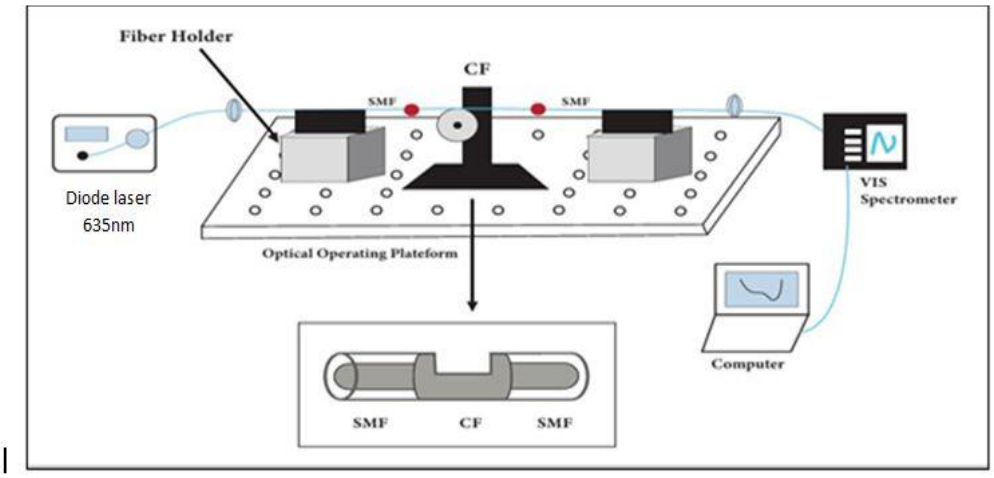

Fig.4: The polishing device to fabricate and characterize the DSCF sensor.

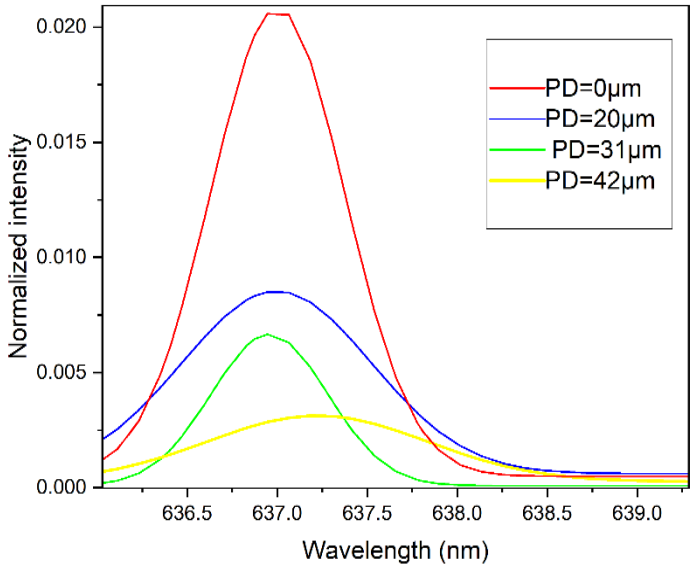

Fig.5: The relation between the intensity and the wavelength with different polishing depths

The middle of CF was placed on a grinding wheel for polishing until the desired depth was achieved, resulting in the fabrication of the DSCF. The peak of the output intensity (I in) was recorded before the DSCF (operating the grinding wheel) at an external RI of air=1. As the grinding wheel operated, the peak of intensity gradually decreased as the polishing duration extended. After turning off the grinding wheel,

the peak of the intensity after DSCF (I out) was recorded, and the remaining intensity was calculated using Eq. 2:

$$\text{The remaining intensity} = (I_{out} / I_{in}) \% \quad (2)$$

To determine the optimal PD experimentally, the first step was repeated three times with three SCS structures. Each time, the polishing period was extended more than the previous period to increase the PD. The output intensity recorded by the spectrometer decreased as the PD increased, as shown in Fig.5. This indicates that there is attenuation in output power because the evanescent wave leaks from the surface of the DSCF structure due to a decrease in the diameter of the CF from one side. This resulted in three different PDs (20 µm, 31 µm, 42 µm) as shown in Fig.6. The remaining intensity was calculated using Equ.3 for each PD of the fabricated DSCF structure.Then, the transmission spectrum was measured by OSA as shown in Fig.7, and the sensitivity was calculated to choose the optimal polishing depth which achieved the highest sensitivity among the three structures, as shown in Fig.8.

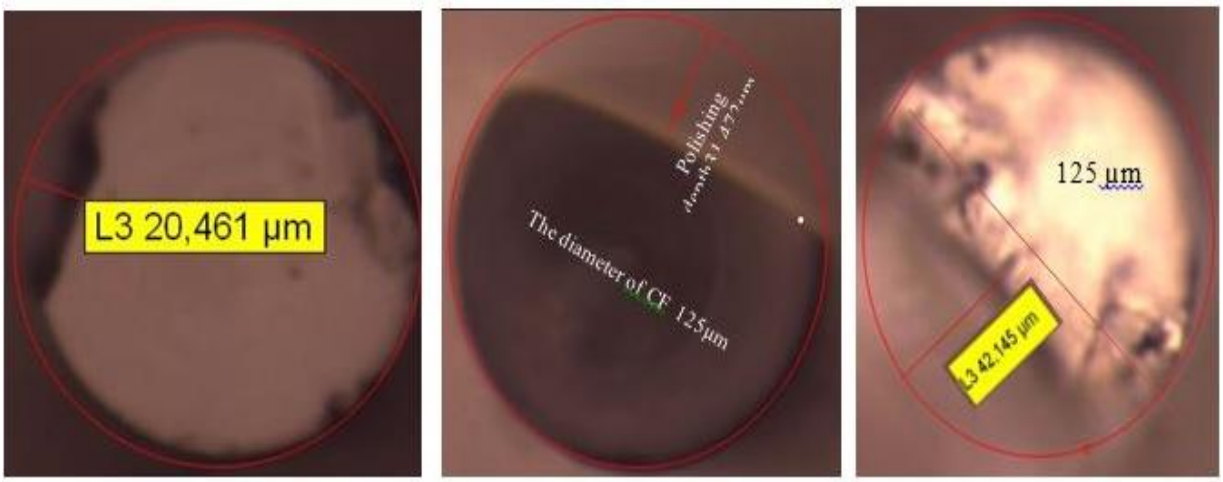

Fig.6: The image under the microscope showed the cross-section of DSCF when PD equal to (a) 20µm, (b) 31µm, and (c) 42µ.

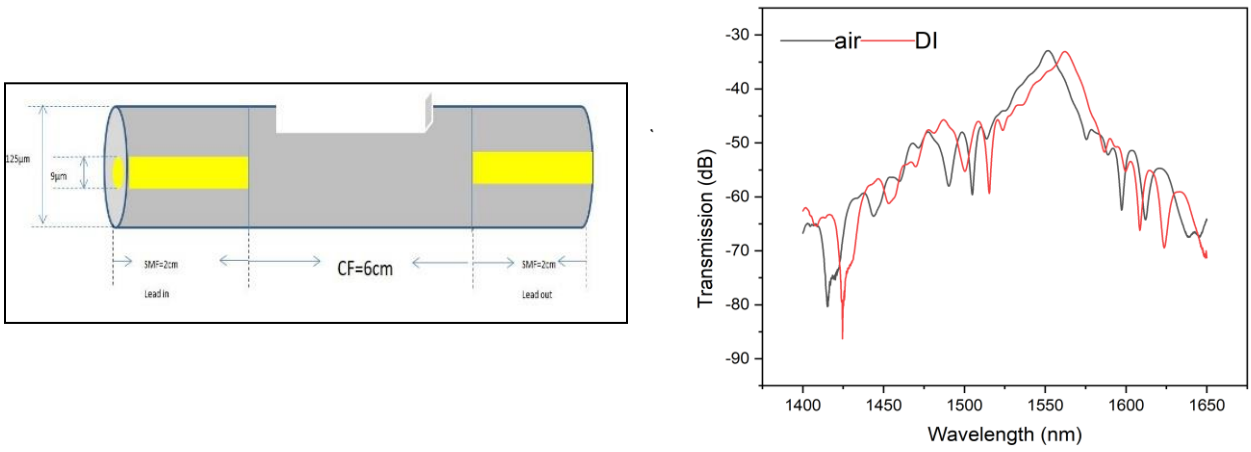

(a) **(b)**

Fig.7: DSCF structure (a)schematic diagram of DSCF structure(b)transmission spectrum of DSCF structure.

3.3 The preparation of Sodium Chloride (NaCl) solution

The NaCl solutions used in this study had concentrations ranging from 5% to 25%. To prepare these solutions, specific amounts of NaCl powder were weighed using an electronic scale and then dissolved in 100 ml of deionized water (DI) at room temperature using a magnetic stirrer. For example, to prepare 5%, 10%, 15%, 20%, and 25% of NaCl solutions, 5g, 10g, 15g, 20g, and 25g of NaCl powder should be added to 100 ml of DI, respectively. The RIs corresponding to these concentrations were demonstrated in Table 1 [32]. The RIs of the prepared solutions were measured by an Abb refractometer to evaluate the sensitivity of this proposed sensor.

Table 1: The refractive indices of the NaCl concentrations.

NaCl Concentrations (%)	DI	5	10	15	20	25
Refractive Index (RIU)	1.33	1.34	1.35	1.36	1.37	1.38

4. The experimental setup

Firstly, one end of the SCS sensor was connected to a broadband source (BBS) with a wavelength range of 1500-1600 nm, and the other end of the sensor was connected to the OSA (YOKOGAWA AQ6370C OSA) to determine the sensitivity of this structure by measuring its transmission spectra before polishing the CF.

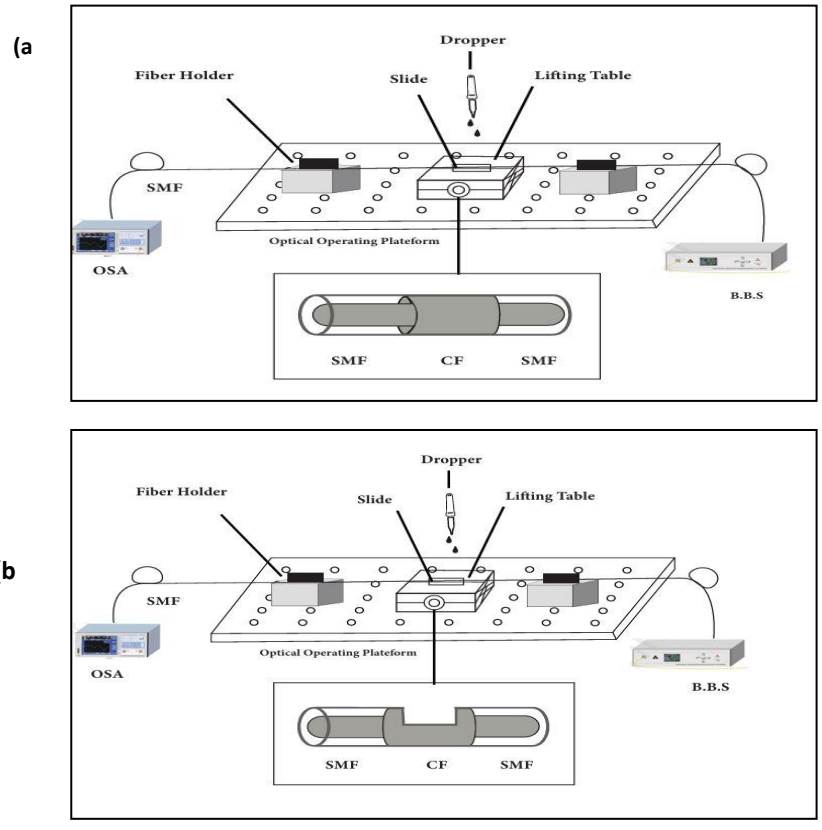

Fig.8: Experimental setup of DSCF RI sensor with different concentrations of NaCl solution by OSA (a) Testing the sensor before DSCF (b) Testing DSCF sensor.

The SCS structure was examined by OSA with different concentrations of NaCl from 5% to 25 % with an increase of 5%. Secondly, after fabrication, the DSCF sensor was connected with OSA from one side and BBS from the other side as present in Fig.8(a) to calculate the sensitivity by OSA for the three different polishing depths with the same previous method and concentrations that were used before the DSCF sensor. This is demonstrated in Fig. 8 (b)

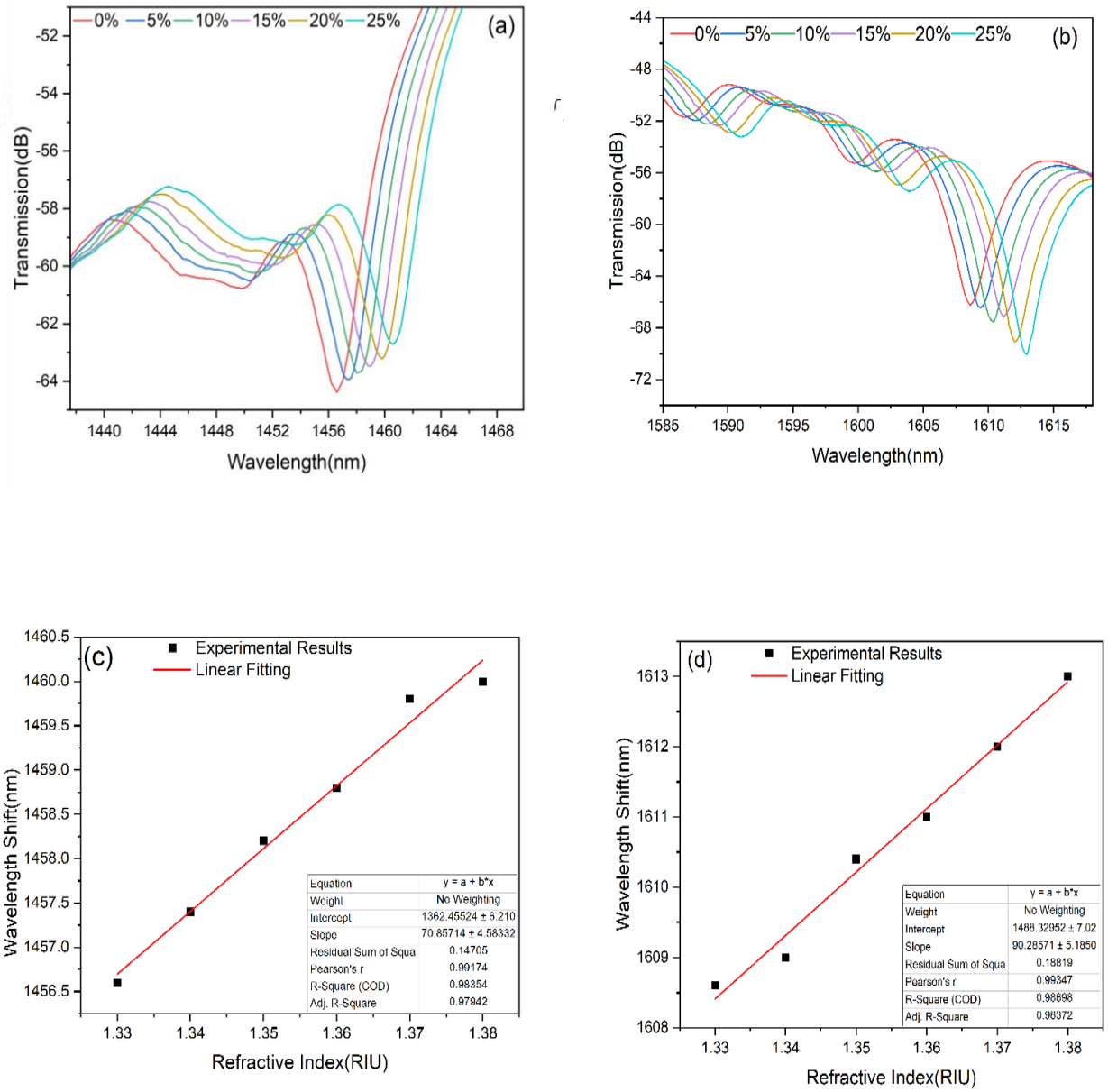

Fig.9: Transmission spectra and sensitivity measured with the different concentrations of NaCl solution respectively ((a), and (c)) before DSCF, ((b), and(d)) after DSCF.

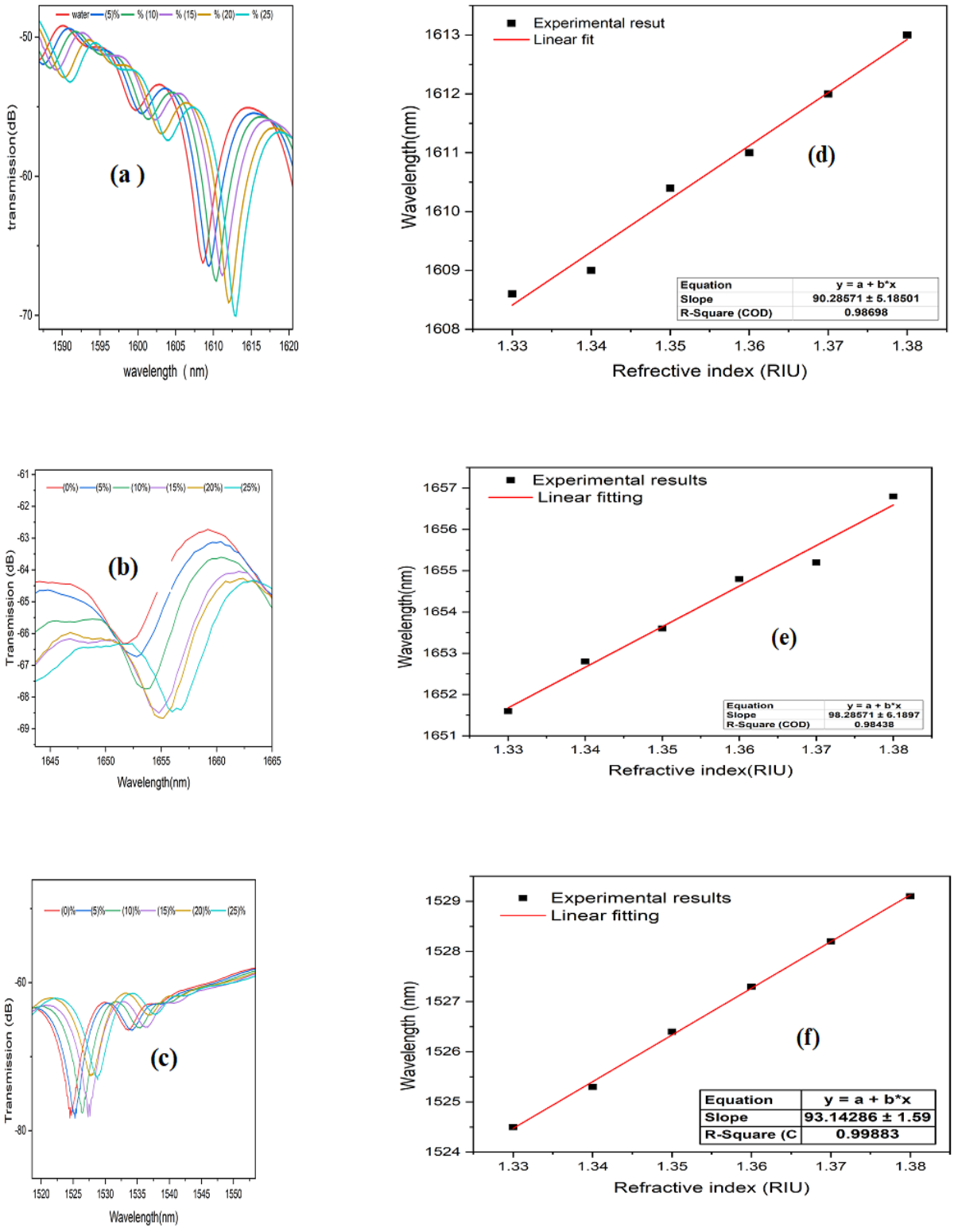

Fig. 10: Transmission spectra recorded by OSA from the measurements of the DSCF sensor with three different PDs (a) for PD=20μm (b) for PD=31μm and (c) for PD= 42 μm. Experimental results of RI when (d) PD=20μm (e) PD=31μm (f) PD= 42

Table 2: The relationship between the remaining intensity and the sensitivity to choose the optimal depth.

Structure Name	Polishing Depth(μm)	(I_{out}/I_{in})%	Sensitivity (nm/RIU)
structure1	20	80	90
structure 2	31	70	98
structure 3	42	42	93.14

was done to prevent any interference from the residual solution on the surface. The SCS sensor was placed on a lifting table and fixed at both ends with fiber holders. The sensing area was placed on the slide, and the NaCl solution was dripped onto the slide until the sensing area was fully immersed. Every step was recorded and fixed, starting with air, so that the spectrum coincided with the previously recorded air spectrum. Each step was recorded and fixed by OSA starting with air to investigate its transmission spectra, and the sensitivity(S) was calculated from the slope between the shift in wavelength and the corresponding RI (n) of each using concentration. This is illustrated in Eq.3 [33]:

$$S = \Delta\lambda_{shift}/\Delta n \quad (3)$$

Where Δλ shift represented the shift in wavelength.

OSA tested the DSCF sensor to measure the transmission spectra shown in Fig. 9 using various RIs of NaCl solutions ranging from 1.33 to 1.38 in increments of 0.01 for each RI measurement. These measurements were taken both before and after the polishing process, with the NaCl solutions replacing air as the cladding. Fig. 9(a) and (b) compare the transmission spectra measured by OSA before and after using the grinding wheel, respectively.

It was observed that several dips will appear in the transmission spectrum due to the MMI in the FCL , Then this dip shifted towards longer wavelengths as the RI of the NaCl solution increased. In Fig. 9 (c), the experimental results show an increase in sensitivity, calculated from the slope of the linear fitting, from 70.8 nm/RIU before the DSCF to 90 nm/RIU after the DSCF as demonstrated in (c) and (d) respectively. In this study, three different PDs were created of 20 μm, 31 μm, and 42 μm. The corresponding sensitivities were 90nm/RIU, 98nm/RIU, and 93.14nm/RIU, respectively, as shown in Fig. 11. When the PD had a depth of 20 μm, the peak of the output intensity decreased, but there was no significant energy loss. Upon increasing the PD depth to 31 μm, the sensitivity increased to 98nm/RIU, indicating the optimal polishing depth. Fig. 10 illustrates the transmission spectra measured by OSA, and the sensitivity calculated from the linear fitting demonstrated that the 31 μm PD achieved the highest sensitivity among the three DSCF sensors, with a good linearity of 9.8. The three polishing depths and their corresponding sensitivities are summarized in Table 2.

It was observed that the linear fitting curve of the experiment after one month is very close to the linear fitting curve of the original experiment, and the sensitivity decreased from 98.2 to 93.7 which confirms that the sensor is with good repeatability which is illustrated in Fig.11. To compare with the proposed structures, Table 3 shows a comparative analysis of the results between the sensors of different structures reported previously.

Table 3: shows a comparative analysis of the results between the sensors of different structures reported previously To compare with the proposed structures.

Structure	RI Range	RI Sensitivity (nm/RIU)	References
Core-offset SMF	1.33-1.374	78.8	[32]
Double tapered SMF	1.348-1.403	68.6	[34]
SCS Structure offset fiber [16]	1.33-1.38	98.768	[16]
Tapered Splicing SMF-PCF-SMF	1.33-1.38	20 pm / RIU	[17]
DSCF SCS Sensor	1.33-1.38	98.2	In this work

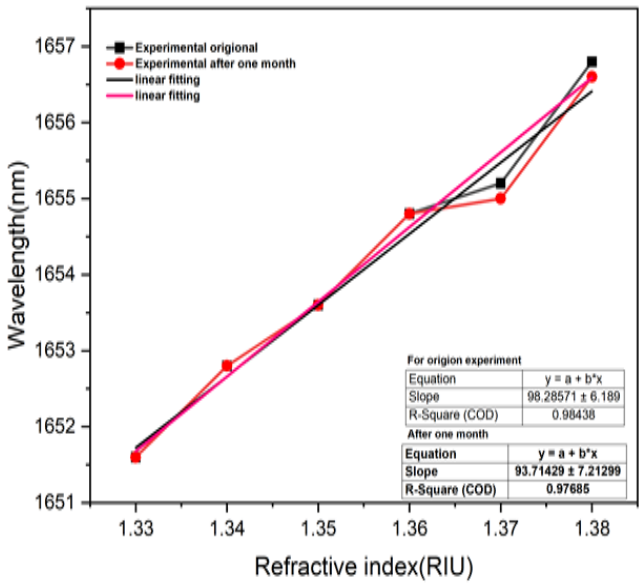

Fig.11: A comparison chart of the original experimental result when the PD was 31µm and the experimental result after one month.

5. Conclusion

A DSCF for RI sensors based on SCS structure has been created using a grinding wheel to improve sensitivity to the surrounding refractive index. Three different DSCF structures with varying polishing depths were fabricated for experimental comparison and their RI sensing characteristics are demonstrate. The optimal polishing depth was 31 µm achieved the highest sensitivity of 70 to 98 nm/RIU for different concentrations of NaCl solution ranging from 1.33-1.38 and the correlation coefficient (R2) was 9.8. Further optimization schemes are under study to enhance the sensitivity. This makes the DSCF sensor suitable for many applications like biosensors and environment pollution, easy to fabricate, good stability, and compact.

References

[1] Keirsse J, Boussard-Pledel C, Loreal O, Sire O, Bureau B, Leroyer P, Turlin B, Lucas J. "IR optical fiber sensor for biomedical applications," (2003). Vib Spectrosc; 32:23–32.

[2] García Esteban-Barcina I, Beloki Perurena J, Zubia Zaballa JA, Aldabaldetreku Etxeberria G, Illarramendi Leturia MA, Jiménez Hernández F. "An Optical Fiber Bundle Sensor for Tip Clearance and Tip Timing Measurements in a Turbine Rig," (2013).
[3] Jha R, Gorai P, Shrivastav A, Pathak A. "Label-Free Biochemical Sensing Using Processed Optical Fiber Interferometry: A Review," (2024). ACS Omega; 9:3037–3069.
[4] Friebele EJ, Askins CG, Bosse AB, Kersey AD, Patrick HJ, Pogue WR, Putnam MA, Simon WR, Tasker FA, Vincent WS. "Optical fiber sensors for spacecraft applications," (1999). Smart Mater Struct; 8:813.
[5] Abbas HK, Mahdi ZF. "D-shape Optical Fiber Development and Enhancement as a Refractive Indices Sensor Using Surface Plasmon Resonance," (2023). Iraqi J Laser; 22:80–90.
[6] Li X, Zhang H, Qian C, Ou Y, Shen R, Xiao H. "A new type of structure of optical fiber pressure sensor based on polarization modulation," (2020). Opt Lasers Eng; 130:106095.
[7] Polygerinos P, Seneviratne LD, Althoefer K. "Modeling of light intensity-modulated fiber-optic displacement sensors," (2010). IEEE Trans Instrum Meas; 60:1408–1415.
[8] Zhang J, Sun Q, Liang R, Wo J, Liu D, Shum P. "Microfiber Fabry–Perot interferometer fabricated by taper-drawing technique and its application as a radio frequency interrogated refractive index sensor," (2012). Opt Lett; 37:2925–2927.
[9] Smetana J, Walters R, Bauchinger S, Ubhi AS, Cooper S, Hoyland D, Abbott R, Baune C, Fritchel P, Gerberding O. "Compact Michelson interferometers with subpicometer sensitivity," (2022). Phys Rev Appl; 18:34040.
[10] Lin W, Shao L, Liu Y, Bandyopadhyay S, Liu Y, Xu W, Liu S, Hu J, Vai MI. "Temperature sensor based on fiber ring laser with cascaded fiber optic Sagnac interferometers," (2021). IEEE Photonics J; 13:1–12.
[11] Mohammed SA, Al-Janabi AH. "All fiber chemical liquids refractive index sensor based on multimode interference," (2018). Iraqi J Laser; 17:33–39.
[12] Liu W, Wu X, Zhang G, Li S, Zuo C, Fang S, Yu B. "Refractive index and temperature sensor based on Mach-Zehnder interferometer with thin fibers," (2020). Opt Fiber Technol; 54:102101.
[13] Wang S, Lv R, Zhao Y, Qian J. "A Mach-Zehnder interferometer-based High Sensitivity Temperature sensor for human body monitoring," (2018). Opt Fiber Technol; 45:93–97.
[14] Wang S, Ma Y, Chen W, Wang S, Yi Y, Li X, Lu C, Zhang S, Geng T, Sun W. "Ultrasensitive strain sensor based on Mach-Zehnder interferometer with bent structures," (2021). J Light Technol; 39:6958–6967.
[15] Hamza N. "Enhanced refractive index sensor based on etched coreless fiber," (2020). Authorea Prepr.
[16] Taher HJ, Mejble AR. "S and U Shape Offset Studying of the Refractive Index Sensor Based on Coreless Fiber," (n.d.).
[17] Salman NA, Taher HJ, Mohammed SA. "Tapered splicing points SMF-PCF-SMF structure based on Mach-Zehnder interferometer for enhanced refractive index sensing," (2017). Iraqi J Laser; 16:19–24.
[18] Bakurov DD, Ivanov OV. "Control of Excitation of Cladding Modes by Tapering an Insertion of Special Fiber," (2021). Sensors; 21:2498.
[19] Dong H, Chen L, Zhou J, Yu J, Guan H, Qiu W, Dong J, Lu H, Tang J, Zhu W, Cai Z, Xiao Y, Zhang J, Chen Z. "Coreless side-polished fiber: a novel fiber structure for multimode interference and highly sensitive refractive index sensors," (2017). Opt Express; 25:5352.
[20] Liu Y, Zhang W, Tong Z, Wang X, Liu D, Wang M, Yu H. "Research on MZI sensor for refractive index and temperature based on D-shaped no core fiber," (2024). Opt Mater (Amst); 148:114933.
[21] Hu C, Wang C, Zhou S, Zhu Z, Wu H, Sun K, Ma X. "Simulation and experimental investigation of the surface morphology formation mechanism of a D-shaped fiber processed using a pulsed CO2 laser," (2022). Opt Laser Technol; 153:108195.
[22] Abbas HK, Mahdi ZF. "D-shape Optical Fiber Development and Enhancement as a Refractive Indices Sensor Using Surface Plasmon Resonance," (2023). Iraqi J Laser; 22:80–90.
[23] Chen M, Lang T, Cao B, Yu Y, Shen C. "D-type optical fiber immunoglobulin G sensor based on surface plasmon resonance," (2020). Opt Laser Technol; 131.
[24] Falah AAS, Wong WR, Mahamd Adikan FR. "Single-mode eccentric-core D-shaped photonic crystal fiber surface plasmon resonance sensor," (2022). Opt Laser Technol; 145.
[25] Liang H, Shen T, Feng Y, Liu H, Han W. "A d-shaped photonic crystal fiber refractive index sensor coated with graphene and zinc oxide," (2021). Sensors (Switzerland); 21:1–16.
[26] De-Jun F, Mao-Sen Z, Liu G, Xi-Lu L, Dong-Fang J. "D-shaped plastic optical fiber sensor for testing refractive index," (2014). IEEE Sens J; 14:1673–1676.
[27] Ballato J, Dragic P. "Glass: the carrier of light-a brief history of optical fiber," (2016). Int J Appl Glas Sci; 7:413–422.

[28] Huang S-C, Lin W-W, Tsai M-T, Chen M-H. "Fiber optic in-line distributed sensor for detection and localization of the pipeline leaks," (2007). Sensors Actuators A Phys; 135:570–579.
[29] Choi S, Eom TJ, Yu JW, Lee BH, Oh K. "Novel all-fiber bandpass filter based on hollow optical fiber," (2002). IEEE Photonics Technol Lett; 14:1701–1703.
[30] Razali NM, Lokman MQ, Zuikafly SNF, Ahmad F, Yahaya H. "Simulation of Self-Image Interference in Single Mode-No-Core-Single Mode Fiber with COMSOL Multiphysics," (2022). J Phys Conf Ser; 2411.
[31] Mejbel AR, Taher HJ. "Coreless fiber length influence for refractive index measurements based on lateral offset structure," (2022). NeuroQuantology; 20:2337.
[32] Zhao Y, Li XG, Cai L. "A highly sensitive Mach-Zehnder interferometric refractive index sensor based on core-offset single mode fiber," (2015). Sensors Actuators A Phys; 223:119–124.
[33] Cennamo N, Massarotti D, Conte L, Zeni L. "Low cost sensors based on SPR in a plastic optical fiber for biosensor implementation," (2011). Sensors; 11:11752–11760.
[34] Yang W, Pan R, Yu X, Fan J, Xiong Y, Wu M. "A high sensitivity asymmetric double tapered fiber interference sensor," (2020). Optik (Stuttg); 210:164495.

تحسين حساسية مستشعر معامل الانكسار بالاعتماد على الالياف عديمة النواة على شكل حرف D

دينا نعمت عبدالله *,حنان جعفر طاهر

معهد الليزر للدراسات العليا، جامعة بغداد، بغداد، العراق

*البريد الالكتروني للباحث: *dina.neamat2201m@ilps.uobaghdad.edu.iq*

الخلاصة

تم تطوير مستشعر لقياس التغير في معامل الانكسار للمحيط باستخدام تقنية مستشعر الألياف غير النواة على شكل حرف(D) . يتكون هذا المستشعر من قطعة من الألياف غير النواة (CF) ملحومة بين ليفين أحادي النمط (SMF). تم تلميع منتصف طول الألياف غير النواة باستخدام عجلة طحن لتقليل القطر من جانب واحد، مما أدى إلى إنشاء مقطع عرضي على شكل حرف D. تم اختبار أداء مستشعر DSCF باستخدام تركيزات مختلفة من محاليل كلوريد الصوديوم (NaCl)، حيث تتراوح معاملات الانكسار (RI) من 1.33 إلى 1.38. تم تحديد عمق التلميع الأمثل (PD) عند 31 ميكرومتر تجريبياً، وتم تحقيق ذلك عن طريق تمديد مدة التلميع باستخدام عجلة الطحن. أدى ذلك إلى زيادة الحساسية من 70.2 نانومتر/وحدة معامل الانكسار إلى 98 نانومتر/وحدة معامل الانكسار، مما يعني أن الحساسية زادت بمقدار 1.4 مرة. يعتبر مستشعر DSCF جهازاً عالي الأداء ومتعدد الاستخدامات وذو تكلفة فعالة مع قدرة قوية على التداخل، وهو مناسب لمجموعة متنوعة من التطبيقات.